PHOTONICS Research

Intracavity-dynamics-based optical phase amplifier with over tenfold amplification

Mingwang Tian and Yidong Tan*

The State Key Laboratory of Precision Measurement Technology and Instruments, Department of Precision Instrument, Tsinghua University, Beijing 100084, China
**Corresponding author: tanyd@tsinghua.edu.cn*

Received 8 May 2023; revised 25 August 2023; accepted 6 September 2023; posted 6 September 2023 (Doc. ID 494882); published 26 October 2023

The relative phase change between two light fields can be used as a fundamental parameter to measure the physical quantity causing this change. Therefore, amplifying the relative phase change becomes attractive to improve the measurement resolution. Phase amplification using a many-body entangled state (NOON state) is a well-known method; nevertheless, the preparation process for a high-number NOON state is difficult and sensitive to optical loss. Here, we propose and experimentally verify a concise phase amplification method with a tolerance of about five orders of magnitude for optical loss. The method is based on the optical-feedback-induced intracavity harmonics generation effect to amplify the phase change by 11 times, which is comparable to the highest level of about 10 experimentally reached in NOON states. Furthermore, the 20th intracavity harmonic is generated when the reinjected photon number increases, indicating that 20 times phase amplification is attainable. The proposed method has a prospect for precision measurement applications.

https://doi.org/10.1364/PRJ.494882

1. INTRODUCTION

Phase is one of the most basic parameters in wave optics and quantum mechanics [1–3]. Phase change between the two arms of the interferometer or in the superposition state of quantum mechanics is very critical because many basic physical quantities can be converted to the detection of the phase change of light, including displacement [4], angle [5], temperature [6], etc. [7,8]. To explore the changing process of these physical quantities, it is often necessary to obtain the relative phase change of the light field in the interferometer. For some ultra-precision measurement, the original phase change is extremely small [9]. For example, in the space gravitational wave detection frequency band, the sensitivity of phase detection is of the order of tens of $\mu\text{rad}/\sqrt{\text{Hz}}$ [10,11]. It should be pointed out that we use the noise spectral density unit commonly used in gravitational wave detection instead of the phase unit (radian); by combining with the signal bandwidth, the minimum phase drift can be further obtained. Therefore, if the phase can be amplified, it will play a key role in improving the phase resolution in the field of precision measurement. The traditional interferometric optical subdivision method increases the detected phase change by increasing the optical path change [12]; however, its essence is not to directly amplify the light phase, but to increase the change of displacement through the relatively complex spatial structure of the optical path.

In quantum optics, there is a well-known method of amplifying phase that is based on a multi-photon number and path entangled state known as the NOON state [13,14], which can be described as $(|N0\rangle_{ab} + |0N\rangle_{ab})/\sqrt{2}$. The NOON state contains N indistinguishable particles in an equal superposition of all being in one of two possible paths a and b [1,15,16]. Phase amplification in this state is a manifestation of the N-photon de Broglie wavelength λ/N [16], and the phase oscillation is N times faster than that of single photon, which results in super-resolution of the phase.

NOON states can be used to amplify phase in ultra-precision measurement, which is very helpful to improve phase resolution [17], but it is usually difficult to prepare a NOON state with a high photon number, and the experimental highest phase amplification in NOON states [17,18] as far as we know is about 10. At the same time, the detection probability will also decrease when N becomes larger, and the NOON state with a high photon number is very sensitive to any optical loss, which increases the difficulty of related experiments. Li *et al.* proposed a novel phase amplification method; they achieved quadruple phase amplification in the harmonic-assisted process, and confirmed that higher magnification phase amplification can be further achieved through cascading [1]. This phase amplification method will play a significant role in the field of precision metrology, and also provides a new idea for phase amplification technology. However, in this method, the high nonlinear conversion efficiency and phase amplification need high pump power and a proper crystal to be successful [1], which leaves room for further improvement.

In this paper, we propose and experimentally verify the effect of a new phase amplification method based on the feedback-induced intracavity harmonic generation (FIHG) effect in a laser frequency-shifted feedback interferometer (LFFI). In our proposed method, the relative phase change between the two arms of the interferometer is amplified by 11 times by the FIHG effect without assistance of any external harmonic generation, which exceeds the maximum magnification of around 10 experimentally obtained by using NOON states; at the same time, in the proposed system, the reflective mirror to losslessly return light in the traditional interferometer can be replaced with a non-cooperative target (non-cooperative means that the target cannot be fitted with a mirror, and great optical loss will occur when the light is scattered by the target), because the system has extremely high weak-light sensitivity, which can respond to the echo optical signal of single-photon order per feedback modulation period. The proposed system also has a tolerance of about five orders of magnitude for optical loss to amplify phase. In addition, we show the possibility that the proposed system can amplify the phase change by 20 times when the number of reinjected photons increases.

The LFFI is different from the traditional Michelson interferometer or Mach–Zehnder interferometer. In the LFFI, the cavity emitting laser irradiates the target, and the backscattered or reflected light of the target returns to the laser cavity and interferes with the intracavity light field, which modulates the light field in the cavity and makes the re-output laser loaded with external information (amplitude, phase, etc.). That is, in the LFFI, the two arms of the interferometer can be regarded as the external cavity light field and the intracavity light field, which leads to the fact that the external returned light is affected by the laser intracavity dynamics while interfering with the intracavity light field, and this will cause some interesting phenomena that are not available in the traditional interference. For example, the returned weak light can be magnified about 10^6 through the intracavity resonance before output again [19], which makes the LFFI avoid dependence on the target mirror and enables it to detect weak signals more easily. Li *et al.* provided a detailed review of laser feedback technology, discussing its principles and applications in the field of metrology [20]. Liu *et al.* reviewed the principles and applications of sensing using laser feedback technology [21]. Lacot *et al.* studied the variation of the relaxation oscillation frequency of a laser cavity in a nonlinear optical feedback state [22], but did not explore the amplification phenomenon of laser phase in a nonlinear state.

Lacot *et al.* found that in a strong feedback state, multiple harmonic peaks appear in the laser power spectrum [23]. Recently, we further found that using this harmonic effect, the relative phase change between the external cavity light field and the intracavity light field can be amplified. It means that we can achieve phase amplification through this FIHG process in the LFFI to obtain phase super-resolution measurement. We will illustrate this phase amplification method from theoretical simulation and experimental verification below.

2. PRINCIPLE AND SETUP

The working schematic diagram of the LFFI is shown in Fig. 1.

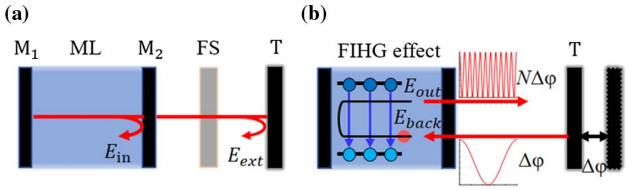

Fig. 1. Working model of the laser frequency-shifted feedback system. (a) Working process of the LFFI. ML, microchip laser; M_1, M_2, resonator mirrors of the ML; FS, frequency-shifter; T, target; E_{in}, light field reflected by M_2; E_{ext}, backscattered light field from the target. (b) Schematic diagram of the phase amplification process of returned light in the LFFI. E_{back}, light field returned to the laser cavity from the target with the phase change of $\Delta\varphi$; E_{out}, re-output light field after phase amplification of N times (here, $N = 11$) by the FIHG effect.

From Fig. 1(a), we can see that the LFFI has the characteristics of optical path self-collimation; the two arms of the interferometer are E_{in} and E_{ext}, which makes it not need to tightly adjust the beam like the Michelson interferometer. The phase carried by the returned light is amplified by the FIHG effect and output again, as shown in Fig. 1(b). Since the feedback interference occurs in the cavity, we can use the intracavity dynamics equations as shown in Eq. (1) to describe the complete interference process [23]:

$$\begin{aligned}\frac{dN}{dt} &= \gamma_1(N_0 - N) - BN|E(t)|^2,\\ \frac{dE(t)}{dt} &= \left[i(\omega_c - \omega) + \frac{1}{2}(BN - \gamma_c)\right]E(t)\\ &\quad + \gamma_c\sqrt{\kappa}E(t-\tau)e^{i(4\pi\Omega t)}e^{-i(\omega+2\pi\Omega)\tau},\end{aligned} \tag{1}$$

where N is the population inversion, γ_1 is the decay rate of the population inversion, $\gamma_1 N_0$ represents the pumping rate, B is the Einstein coefficient, $E(t)$ is the complex amplitude of the electric field in the laser cavity, ω_c is the laser cavity frequency at the atomic frequency, ω is the optical running laser frequency, γ_c is the decay rate of the photon inside the cavity, κ is the equivalent reflectivity of the external cavity, and the smaller κ represents the greater external optical loss. τ is the transit time of the photon in the external cavity, and $\tau = 2nL_{ext}/c$; here, n is the external cavity medium refractive index, L_{ext} is the external cavity length, and c is the speed of light in vacuum. Ω is the one-way frequency shift of the light provided by the frequency-shifter.

When κ is small (typically less than 10^{-12}), the laser exhibits an effect similar to heterodyne interference, and the output light power can be described as

$$\frac{\Delta I}{I} = \sqrt{\kappa}G(2\Omega)\cos(4\pi\Omega t - \varphi_0 + \Delta\varphi), \tag{2}$$

where ΔI is the intensity modulation of the measurement signal, I is the steady laser output power without feedback, and $G(2\Omega)$ is the gain caused by the feedback interference effect (typically reaches 10^6), which the traditional interference process does not have. φ_0 is the initial fixed phase of the system, $\Delta\varphi$ is the relative change of phase between the two arms in the LFFI and we can demodulate $\Delta\varphi$ through the lock-in amplifier. However, as κ increases, the laser cavity enters a medium

feedback state. Different from the weak dynamic balance adjustment process in the laser cavity under weak feedback, at this time, the external reinjected photons will also cause a strong resonance effect of the intracavity laser. In this process, the energy of the interference fundamental wave will be transferred to the higher-order harmonics in turn, and the order and intensity of the output harmonics depend on the energy of the returned photons. From the perspective of the intracavity dynamics equations, it means that multiple solutions are allowed in the cavity at this time, and the phase oscillation speed of the Nth-order solution is naturally N times faster than that of the fundamental wave representing the original phase change. We demonstrate this FIHG phenomenon by simulating Eq. (1) to obtain the frequency spectra of the laser at different κ, as shown in Fig. 2.

During the simulation process, we set the relative pump level η (ratio of actual pump power to threshold pump power, $\eta = BN_0/\gamma_c$) to 1.6. Moreover, the decay rate of the population inversion γ_1 is set to be 1.11×10^4 s^{-1}, the decay rate of the photon inside the cavity γ_c is set to be 2.75×10^{10} s^{-1}, and the one-way frequency shift of the light Ω is set to be 0.5 MHz. From Fig. 2(a), we can see that in the weak feedback state ($\kappa < 10^{-12}$), there is a single beat frequency peak at 1 MHz representing the interference signal in the laser output frequency spectrum, as well as the inherent relaxation oscillation frequency peak at about 2.1 MHz of the laser, and when κ is of the order of 10^{-12} to 10^{-7}, there are different orders of harmonics of the interference signal appearing in the frequency spectra as shown in Figs. 2(b) and 2(c), and the intensity of harmonics increases with the increase of κ. The light intensity output of the Nth harmonic can be expressed as

$$\frac{\Delta I_N}{I} \propto C_N \cos[N(4\pi\Omega t - \varphi_0) + N\Delta\varphi)]. \quad (3)$$

Here, ΔI_N is the intensity modulation of the Nth harmonic, and C_N represents the intensity output coefficient of the Nth harmonic, which is related to the external optical loss.

Similar to the second-harmonic generation processes utilized in the polarized interferometer [1], in the FIHG effect, the phase carried by the fundamental wave is simultaneously transmitted to the higher harmonic in multiples, which means that we can obtain phase changes of different magnification rates at different levels of harmonics at the cavity output. The dependence on $N\Delta\varphi$ instead of $\Delta\varphi$ allows us to achieve phase super-resolution measurement, because the phase oscillation is N times faster than the original phase change. Next, in order to demonstrate the process of realizing phase amplification by nonlinear LFFI, we build a complete system of the LFFI, whose structure is shown in Fig. 3.

In the LFFI, the phase amplification module is the laser cavity itself. The laser source we use is a 1064 nm Nd:YVO_4 microchip laser with an output power of 5 mW. The laser resonator is formed by a 3 mm × 3 mm × 0.75 mm Nd:YVO_4 crystal plate with the coating on both surfaces. The surface near the pump light is coated to be antireflective at the pump wavelength of 808 nm and highly reflective ($R > 99.8\%$) at the lasing wavelength of 1064 nm, and the output surface is coated with 5% transmittance at a wavelength of 1064 nm. The pump light is a fiber-coupled single-mode laser diode, which is focused onto the center area of the Nd:YVO_4 crystal to produce the laser. The Nd:YVO_4 microchip laser can work at room temperature and pressure. The laser emitted by the Nd:YVO_4 microchip is first divided into two beams by a BS. The transmitted light is collimated by a lens, and differentially shifted by AOM1 and AOM2 (CAFS-070/1-010-TEC-1064-AF-A17, CASTECH). Here, we set the value of the frequency shift Ω to 1 MHz. Then, it irradiates the target and the backscattered light returns to the laser cavity through the original path, and in this process, the light passes through the AOMs once again, so the round-trip frequency shift is 2Ω (2 MHz). The feedback light is loaded with the phase change information caused by the external physical quantity, and this phase change is amplified by the intracavitary FIHG effect. Next, the laser exits the cavity again and is reflected by the BS into the PD. The PD

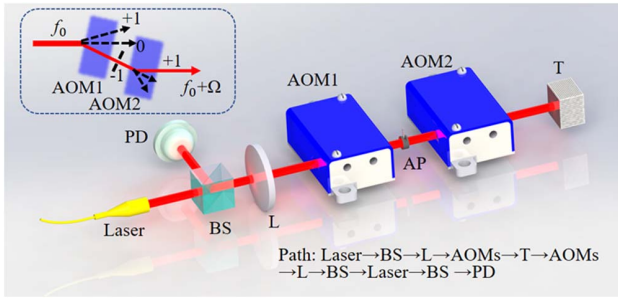

Fig. 3. Schematic diagram of the experimental setup. BS, 7:3 (transmittance:reflectivity) beam splitter; L, convex lens; AOM1, 2, acoustic-optic modulators to provide frequency shift Ω of external light; f_0, laser frequency; AP, aperture; T, target; PD, photodiode.

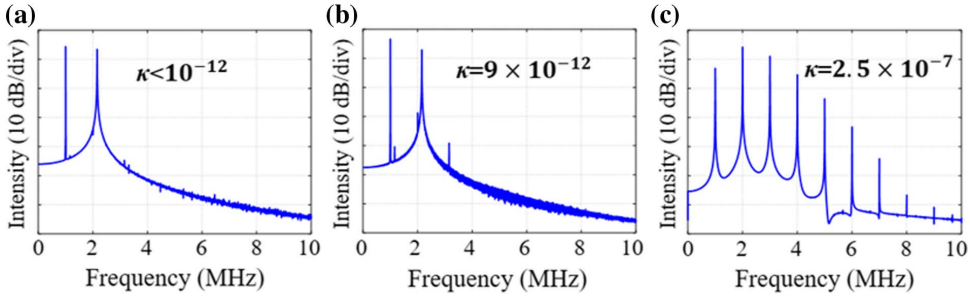

Fig. 2. Frequency spectra of the output laser after feedback interference under different external optical loss states (different κ) with external modulation frequency shift of 1 MHz. (a) $\kappa < 10^{-12}$. (b) $\kappa = 9 \times 10^{-12}$. (c) $\kappa = 2.5 \times 10^{-7}$.

converts the optical signal into an electrical signal in real time and sends it to the lock-in amplifier (HF2LI, Zurich Instruments) to extract the phase information. The specific signal demodulation process diagram is shown in Fig. 4.

As shown in Fig. 4, the driving signal of the AOMs and the detected signal received by the PD are sent into the reference terminal and signal terminal of a lock-in amplifier, respectively. In the signal from PD, the frequencies of all levels of harmonics representing phases with different magnifications are included. Therefore, to obtain an N-fold amplified phase change, we first convert the reference electrical signal driven by AOMs into an N-multiple frequency, which is easy to achieve for electrical signals; then, the signal from PD and the signal from AOMs pass through a mixer and low-pass filter, the high-frequency part is filtered out, and I/Q items are operated by an arctangent function to get the corresponding phase change after N-fold amplification. By writing a program to directly control the lock-in amplifier, we can obtain the phase change after amplification in real time.

In our proposed method, we directly obtain the phase through quadrature phase-sensitive detection, rather than observing the changes in light intensity detected by the photodetector to calculate the oscillation period and restore the phase, which is used in the NOON state method. Compared with the phase acquisition method adopted in the NOON state method, the proposed method has advantages of precise traceability of the phase and resistance to light intensity drift, thus promising a high accuracy for the amplified phase measurement. In addition, since the lock-in amplifier allows multiple groups of reference signals to be input at the same time, we only need to input the AOM signals into the lock-in amplifier after different frequency multiples, so that the phase changes of different magnifications can be obtained simultaneously without changing the optical path structure.

We use a common aluminum block instead of the mirror placed in the traditional Michelson interferometer as the target, and put it at a distance of about 0.5 m from the LFFI. At this time, the backscattered light from the surface of the aluminum block reinjects to the laser cavity, which induces the generation of harmonics in the cavity. The specific experimental results are as follows.

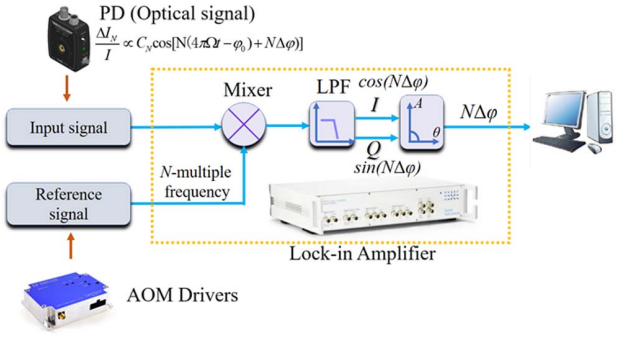

Fig. 4. Flowchart showing the signal processing process of obtaining amplified phase change through lock-in amplifier. Mixer, frequency mixer; LPF, low-pass filter; I, in-phase component; Q, quadrature component; A, θ, amplitude and phase of the signal, respectively; $N\Delta\varphi$, phase output after N-fold amplification.

3. RESULTS

When the intracavity light field is modulated by the light scattered back by the external aluminum block, we can observe the laser output from the fundamental wave to the 11th harmonic on the frequency spectrum analyzer. Figures 5(a)–5(k) show the corresponding frequency spectra of the fundamental wave to the 11th harmonic. It should be noted that due to the small frequency deviation of the AOMs, the frequency of the fundamental wave is 1.9995 MHz rather than perfect 2 MHz, which results in the center frequency of higher harmonics being an integral multiple of 1.9995 MHz.

The aluminum block is placed on the precision displacement stage, whose movement will change the optical path difference (OPD) to change the phase of the light. First, we show the result of the change of the phase without unwrapping with the OPD change of 2 μm in Fig. 6, which can intuitively show the periodic change of the phase oscillation after amplification under the FIHG effect.

The y-axis and x-axis in Fig. 6(a) represent the phase change without unwrapping and the OPD change, respectively. In Fig. 6(a), we can see that the phase oscillation period under the FIHG effect decreases to 1/4 of the original period. For the phase changes that are not amplified or are amplified, the graph presents a periodic serrated curve. In theory, the period of each serration represents a perfect 2π phase change, as shown in Fig. 6(a). The numbers marked on each serration represent the corresponding phase change period for the original or amplified phase change. In Fig. 6(a), the original phase change has only one complete cycle (one complete serration), while the phase change after magnification has six complete cycles (six complete serrations). For the original phase change, we obtain the actual change value of 1.9993π for one cycle, with an error relative to the theoretical value of 0.0007π and an error rate of 0.035%. For the amplified phase, we also calculate the actual phase change value for each cycle, as shown in Fig. 6(b), and we can get that for the amplified phase, the maximum phase deviation in all cycles is 0.0196π and the average phase deviation is 0.0102π. The maximum deviation rate and the average deviation rate are 0.98% and 0.51%, respectively.

Although the phase without unwrapping can more intuitively represent the result of phase oscillation, in the actual precision measurement, we usually need to obtain the unwrapped phase. After unwrapping, the phase change $\Delta\varphi$ is theoretically linearly proportional to the OPD change ΔL, as shown in Eq. (4):

$$\Delta\varphi = N\frac{2\pi}{\lambda}\Delta L, \qquad N = 1, 2, 3\ldots \tag{4}$$

Here, N represents the phase amplification coefficient, and λ is the wavelength of the laser.

Therefore, next, we use the unwrapped phase change to fully demonstrate the ability of the nonlinear LFFI to amplify the phase. The interference results of different harmonics are demonstrated in Figs. 7(a)–7(d), which show the comparison results of the original phase change with two, four, eight, and eleven times amplified phase changes, respectively.

The y-axis and x-axis in Fig. 7 represent the unwrapped phase change and the OPD change, respectively, and the slope

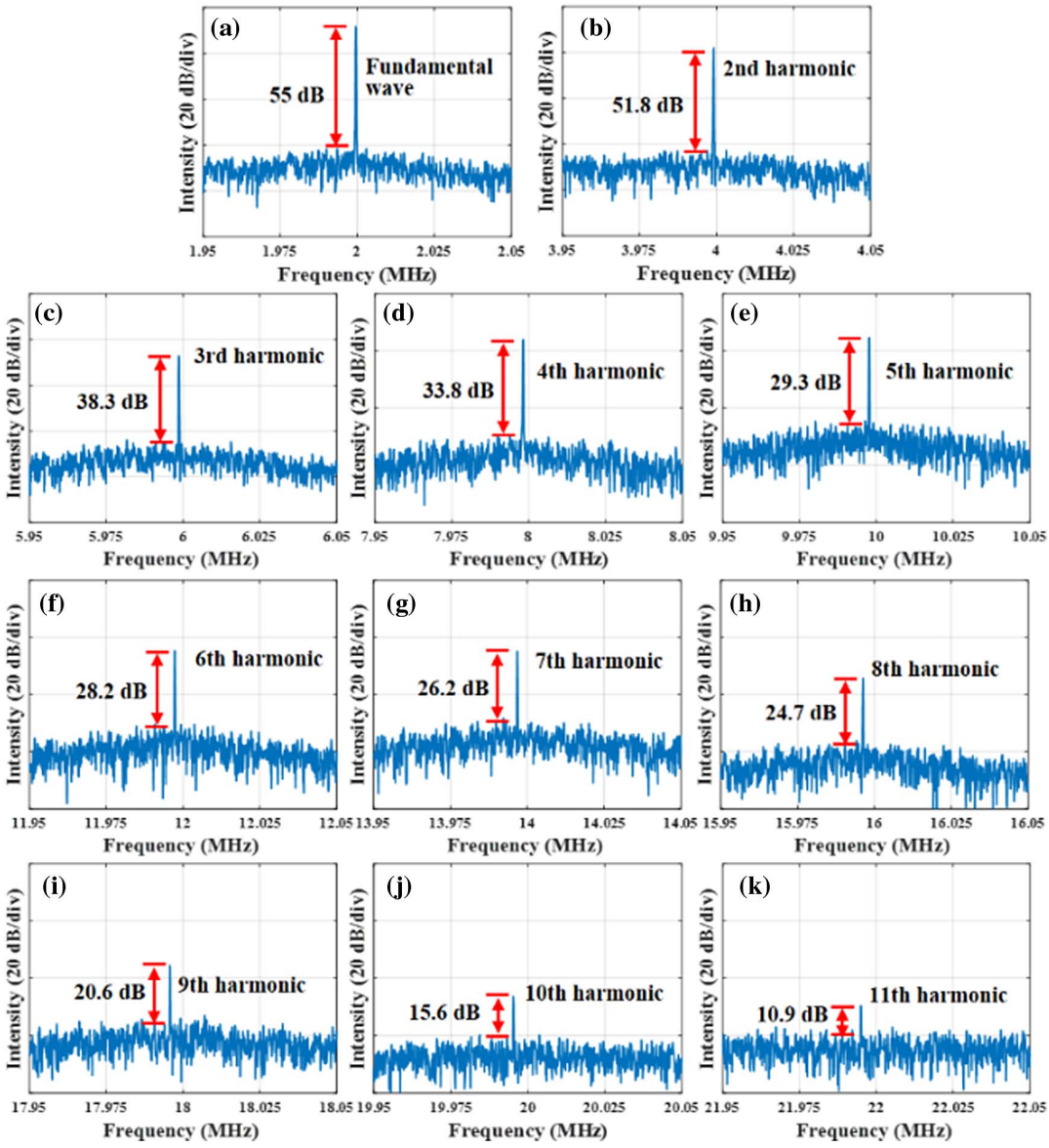

Fig. 5. Corresponding frequency spectra of different harmonics in laser cavity, with corresponding SNR of each spectral peak marked in each subfigure. (a) Fundamental wave. (b)–(k) Second through eleventh harmonics.

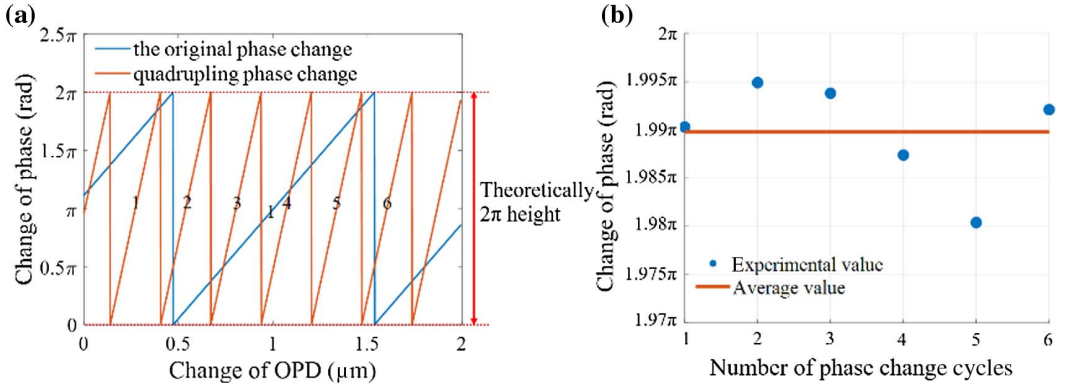

Fig. 6. Schematic diagram of phase amplification result and measurement values. (a) Result of the original phase change and quadrupling phase change without unwrapping. (b) Actual value of the phase change in each cycle after amplification and the average phase change value.

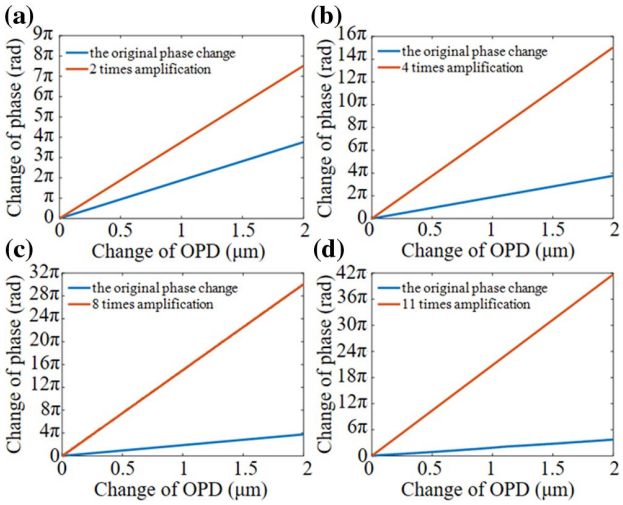

Fig. 7. Comparison of the original unwrapped phase change with two, four, eight, and eleven times amplified unwrapped phase change. (a) Two times amplification. (b) Four times amplification. (c) Eight times amplification. (d) Eleven times amplification.

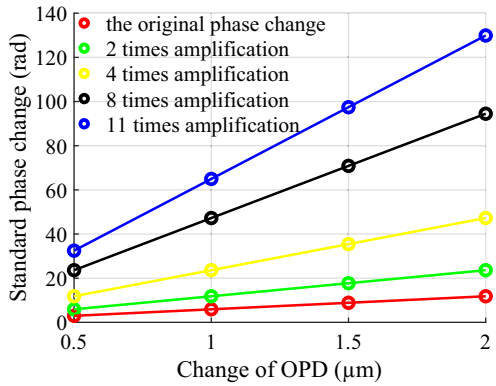

Fig. 8. Theoretical standard phase values corresponding to different OPDs (0.5 μm, 1 μm, 1.5 μm, 2 μm) at different magnifications.

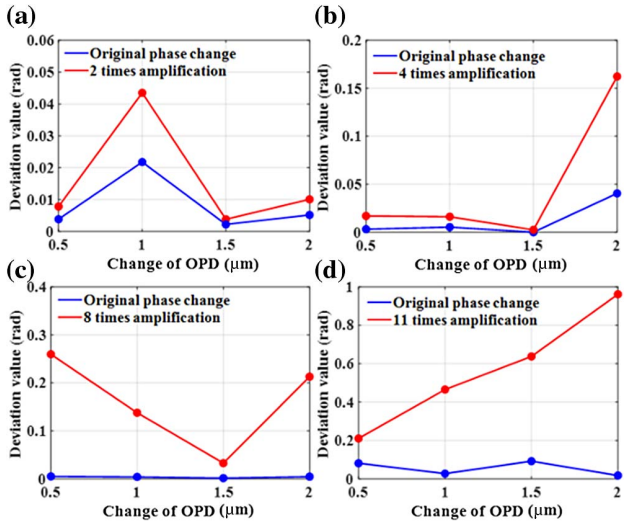

Fig. 9. Errors between measured values and standard phase values corresponding to different OPDs (0.5 μm, 1 μm, 1.5 μm, 2 μm) at different magnifications. (a) Two times amplification. (b) Four times amplification. (c) Eight times amplification. (d) Eleven times amplification.

of each curve represents the corresponding phase change rate. We use the phase change of the fundamental wave of the LFFI to obtain the OPD. When the displacement stage moves, the optical length path changes, causing the phase of the LFFI to change accordingly. According to Eq. (4), we can directly convert the phase into the OPD. Moreover, by utilizing the multi-channel demodulation function of the lock-in amplifier, we can simultaneously obtain amplified phase information through other channels, which ensures that all phase information is obtained in the same OPD change. Using the set displacement value (1 μm) of the displacement stage as the standard value, the deviation between the measured value and the standard value is about 4 nm. From Fig. 7, we can see that the LFFI can produce 11 times phase amplification through the FIHG effect when the target is non-cooperative.

To evaluate the phase errors, we take the corresponding phase values for OPD change values of 0.5 μm, 1 μm, 1.5 μm, and 2 μm in each sub-figure in Fig. 7 for error analysis. Based on Eq. (4), we can theoretically obtain the corresponding standard phase values at different OPDs, as shown in Fig. 8.

By combining the phase values of each point in Figs. 7 and 8, we can obtain the phase errors at different positions, as shown in Fig. 9.

As shown in Fig. 9, we can calculate the maximum deviation rates [(deviation/standard value) × 100%] of the original phase measurement and the phase measurement after two, four, eight, and eleven times magnification, which are 0.37%, 0.37%, 0.34%, 1.10%, and 0.74%, respectively.

In order to further prove the application potential of the phase amplification method based on the FIHG effect in the field of precision metrology and other fields, we carry out the phase amplification experiment for a non-cooperative target at a long distance. The physical device of the experiment and the results of the phase amplification are shown in Fig. 10.

The aluminum block is placed about 130 m away from the LFFI, whose output light power is 10 mW. In this case, the light energy E_r received by the LFFI returned from the target in each feedback modulation cycle is about 1.216×10^{-18} J, which is equivalent to seven photons' energy. The specific calculation method of evaluating the received energy can be seen in Appendix A. At this time, we confirm that the proposed nonlinear LFFI can still achieve four times phase amplification, as shown in the Fig. 10(c). Moreover, if the light collecting system can be further improved, which is equivalent to increasing the effective reflectivity of the external cavity, we can achieve higher magnification phase amplification.

In addition, in the above experiments, the targets we detect are all non-cooperative targets, which means higher external optical loss than that brought by cooperative targets such as reflective mirrors. Nevertheless, it does not mean that the LFFI cannot detect cooperative targets; in some scenarios where reflective mirrors can be used, the optical loss caused by the

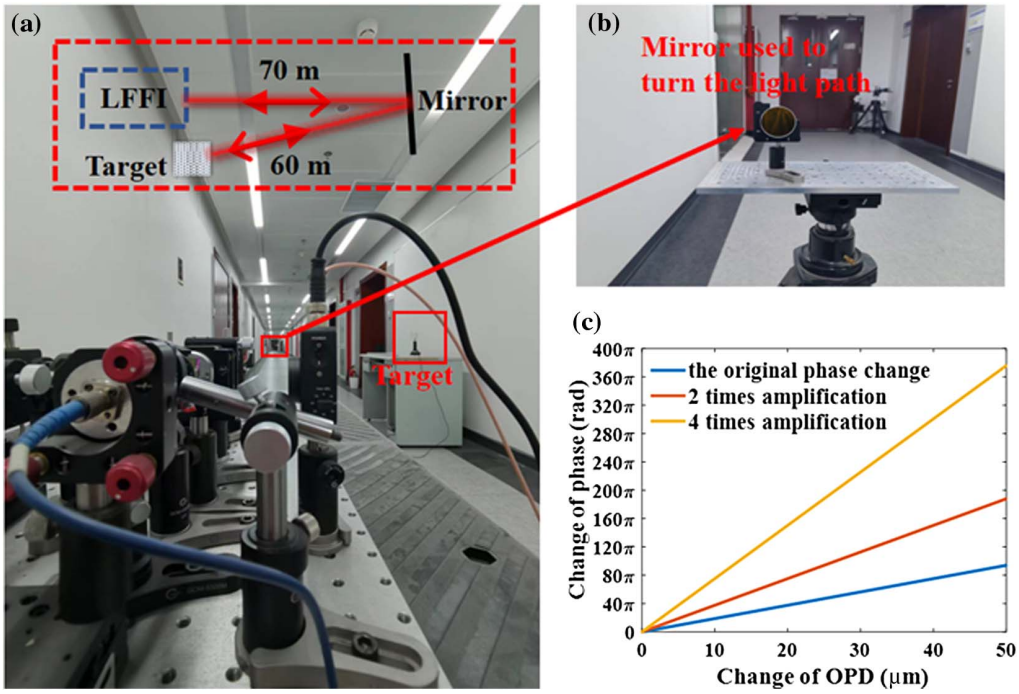

Fig. 10. Physical device of the long-distance experiment and the results of phase amplification. (a) Diagram of the experimental system and the target (aluminum block) in the corridor; inside the red frame is the overall schematic diagram of this long-distance experiment. (b) Diagram of the mirror used to turn the light path, which makes distance from the target to the LFFI reach 130 m. (c) Result of the phase amplified by two times and four times.

reflector can be negligible, and at this time, more feedback photons will excite a more intense harmonic effect in the laser cavity to induce higher-order harmonics, which also means we can achieve higher magnification of phase change. So, next we replace the aluminum block with a reflective patch as the measured target and rotate it by an angle to prevent the cavity from entering a chaotic state due to the strong feedback light, at which point we observe harmonics of up to 20 times in the output frequency spectrum of the laser, which is shown in Fig. 11.

It shows us the possibility of the LFFI to provide 1/20 phase super-resolution measurement under the application scenarios

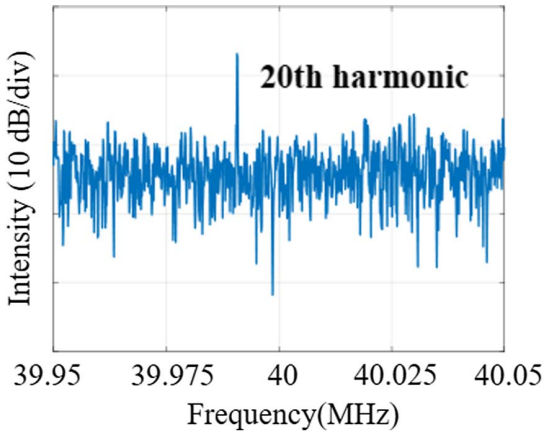

Fig. 11. Corresponding frequency spectrum of the 20th harmonic in laser cavity.

of traditional interferometers such as Michelson and Mach–Zehnder.

4. DISCUSSION AND CONCLUSION

We propose a method that can amplify the relative phase change in laser interferometry based on the FIHG effect. We achieve 11 times phase amplification in the proposed nonlinear LFFI by demonstrating the magnification of the phase change rate to 11 times the original change rate (equivalent to changing the period of phase change to 1/11 of the original period). In our demonstration experiments, the phase change is caused by the OPD change. In fact, as long as the phase information can be loaded into the light, regardless of the physical quantity that causes the phase change, we can perform super-resolution measurements of the phase through the FIHG effect. In addition, we verify that the proposed system also has a phase amplification ability for weak signals returned by long-range non-cooperative targets, which indicates that it has a wide range of application scenarios for most real-world targets that cannot be measured by installing reflective mirrors.

Below, we will discuss the impact of the signal-to-noise ratio (SNR) of harmonics on demodulation. From the SNR of different harmonic peaks marked in Fig. 5, it can be seen that for higher-order harmonics, the SNR decreases gradually compared with the fundamental wave. This decrease in SNR has certain limitations on obtaining the amplified phase. We will explain this below.

The theoretical expression for the SNR of the Nth harmonic generated due to the FIHG effect can be described as [23]

$$\mathrm{SNR}_N = \frac{P_N}{2h\nu\Delta F}. \tag{5}$$

Here, P_N and ΔF represent the power possessed by the Nth harmonic and the demodulation bandwidth, respectively, h is Planck's constant, and ν is the frequency of the used laser. When the initial laser power of the LFFI and the reflectivity of the measured target are determined, the power possessed by the Nth harmonic can be considered deterministic. As the order increases, the harmonic power will decrease, leading to a decrease in the SNR, which is consistent with the results shown in Fig. 5. On the other hand, the SNR and the demodulation bandwidth ΔF of the LFFI are inversely proportional, and ΔF needs to be no less than the Doppler frequency shift f_d caused by the target motion ($\Delta F \geq f_d$), in order to ensure that the system can accurately obtain all phase changes generated when the target moves. The Doppler frequency shift f_d can be determined by Eq. (6):

$$f_d = \frac{2v}{\lambda}. \tag{6}$$

Here, v is the speed of the target's movement, and λ is the laser's wavelength. By analyzing Eq. (6), it can be concluded that f_d is directly proportional to the velocity of the target's motion (this represents the velocity of phase change from the perspective of phase change). In other words, for a target with higher motion speed (higher phase change speed), the generated f_d is larger, and the required ΔF is larger. However, the larger the ΔF, the smaller the SNR. By combining Eq. (5) and Eq. (6), it can be concluded that for the higher-order harmonic, the SNR is reduced compared to lower-order harmonics (under the same demodulation bandwidth), so the system demodulation bandwidth variation it can tolerate is smaller. This means that the target motion speed (phase change speed) it can respond to is smaller, because when the target's motion speed increases, ΔF must also increase accordingly. For higher-order harmonics, the SNR will reach 0 dB earlier than the fundamental wave, making it impossible to accurately obtain phase changes. Therefore, when using the proposed method for phase amplification, the required demodulation bandwidth should be evaluated based on the target motion speed to ensure that all phase information can be accurately obtained when being N times amplified.

In addition, in terms of the relationship between phase demodulation precision and SNR, due to the reduced SNR of higher-order harmonics, the noise in nearby frequency bands is more likely to affect demodulation, leading to a decrease in accuracy. However, since the phase demodulation method we use is quadrature phase-sensitive detection, compared to the commonly used method in NOON states that directly judges phase changes based on changes in light intensity, the quadrature phase-sensitive detection method has a lower requirement for the SNR; therefore, using a lock-in amplifier for demodulation can effectively reduce the adverse effects of the SNR reduction, but this still requires a stable SNR higher than 0 dB within the demodulation bandwidth of the lock-in amplifier.

In summary, due to the different SNRs of different levels of harmonics, the maximum target motion speed (phase change speed) that they can respond to is different. The higher the order, the higher the phase magnification, and the lower the SNR (under the same demodulation bandwidth). The maximum phase change speed that the higher-order harmonic can respond to is lower. Therefore, in practical use, it is necessary to determine the required demodulation bandwidth based on the phase change speed, and to determine the maximum phase magnification that can be obtained under the premise of correctly obtaining phase information.

On the other hand, when the reflector is allowed to be used, we show the potential of the nonlinear LFFI to amplify the relative phase change by 20 times, which exceeds the maximum phase magnification currently achievable in the NOON state. And in our experiments, the lasers used are all low-power lasers. By further increasing the output power of the laser to increase the upper limit of the nonlinear harmonic effect in the cavity, or integrating the optical amplifier to the LFFI to obtain a larger number of reinjected photons, we may be able to get more times of phase amplification. A possible LFFI structure with adding an optical amplifier is shown in Fig. 12, and the path of the beam is ML → L → NPBS1 → ISO → NPBS2 → M1 → OA → AOM1 → AOM2 → M2 → NPBS3 → T → NPBS3 → NPBS1 → L → ML → L → NPBS1 → ISO → NPBS2 → PD. Although it increases the complexity of the system, the number of the reinjected photons can be greatly improved in theory with the integration of the optical amplifier, and greater phase amplification through the FIHG effect in the cavity can be achieved.

Moreover, the proposed phase amplification method has the advantage of detecting the phase change in real time through ordinary photodetectors compared to the method based on the NOON state, which always requires a single photon detector to take a long time in the coincident measurements [24,25]. Furthermore, our system has an optical loss tolerance of up to five orders of magnitude, which makes it able to amplify both amplitude and phase for extremely weak signals, and the proposed FIHG process occurs in the laser cavity, which means that we do not need to set additional nonlinear modules in the system to achieve phase amplification. This has certain advantages over the phase amplification method based on the

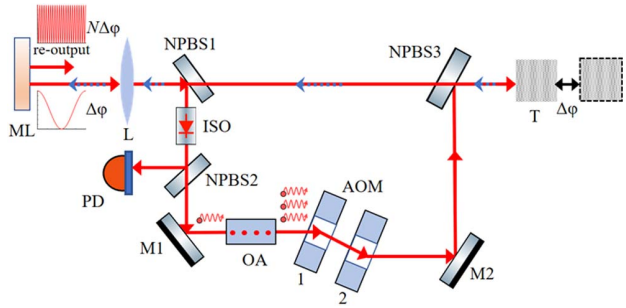

Fig. 12. Schematic diagram of the circular LFFI with adding optical amplifier to get greater phase amplification. ML, microchip laser; L, lens; NPBS1–3, non-polarizing beam splitters with ratios of transmittance to reflectivity of 5:5, 7:3, 5:5, respectively; ISO, optical isolator; M1, 2, mirrors; OA, optical amplifier; AOM1, 2, acoustic-optic modulators to provide frequency shift of external light; T, target; PD, photodiode.

three-wave mixing process, which depends on a certain efficiency of the nonlinear processes [1].

The unique advantage of our proposed scheme is that after the nonlinear LFFI phase amplifier, the external change corresponding to a phase oscillation period is much smaller than that before the amplification. At the same time, the cost of achieving this phase super-resolution effect is rather small compared with the method based on the NOON state [26,27] or based on the harmonic assistance [1]. We believe that the proposed phase amplifier could be widely used in many precision measurement fields, such as measurements of the precision displacement [28] and medium refractive index [29] to improve the measurement resolution, or in the imaging process to improve the imaging resolution [30], or to provide auxiliary analysis assistance for other fields that need to track and study optical phase change [31,32]. The proposed method will greatly change our understanding of nonlinear interference, and may provide a concise approach of super-resolution precision measurement.

APPENDIX A: METHOD FOR EVALUATING THE LIGHT ENERGY RECEIVED BY THE LFFI

In the case of long-distance measurement, we can get the light energy E_r received by the LFFI returned from the target in each feedback modulation by the following equation:

$$E_r = P_0 \eta^2 \Omega_r T / \Omega_0. \tag{A1}$$

Here, $P_0 = 10$ mW is the output power of the laser; $\eta = \eta_{\mathrm{BS}} \eta_{\mathrm{AOMs}} \eta_{\mathrm{lens}}$ denotes the one-way light transmittance of the system ($\eta_{\mathrm{BS}} = 0.7, \eta_{\mathrm{AOMs}} = 0.49, \eta_{\mathrm{lens}} = 0.985$). The total transmittance is η^2 for the light passing through the system twice. $\Omega_r = A_r / L^2$ is the entrance pupil angle of the LFFI, $A_r = \pi r_0^2$ is the receiving aperture area of the system, and $r_0 = 6$ mm is the outgoing spot radius of the system. $L = 130$ m is the distance from the LFFI to the target. $T = 1/f$ is the feedback modulation period, and $f = 2$ MHz is the feedback modulation frequency. $\Omega_0 = \pi$ is the backscattering angle of the measured target (assuming that it is full-angle scattered).

Substituting all the parameters, we get $E_r = 1.216 \times 10^{-18}$ J, which is equivalent to seven photons' energy per feedback modulation cycle. It means that the proposed nonlinear LFFI can respond to extremely weak optical signals and amplify their phase change, which gives it broad application scenarios in the field of precision measurement.

Funding. Tsinghua Initiative Scientific Research Program (2021Z11GHX002).

Acknowledgment. We gratefully acknowledge Prof. Sun for providing guidance in writing this paper. We also sincerely thank Xin Xu and Mingfang Li for providing suggestions on the image format.

Disclosures. The authors declare no conflicts of interest.

Data Availability. The data that support the findings of this study are available from the corresponding author upon reasonable request.

REFERENCES

1. W.-Z. Li, C. Yang, Z.-Y. Zhou, Y. Li, Y.-H. Li, S.-J. Niu, Z. Ge, L. Chen, G.-C. Guo, and B.-S. Shi, "Harmonics-assisted optical phase amplifier," Light Sci. Appl. **11**, 312 (2022).
2. S. Choi, Y. Bao, X.-L. Qi, and E. Altman, "Quantum error correction in scrambling dynamics and measurement-induced phase transition," Phys. Rev. Lett. **125**, 030505 (2020).
3. Y. Fan, J. Sun, Y. Shu, Z. Zhang, Q. Chen, and C. Zuo, "Accurate quantitative phase imaging by differential phase contrast with partially coherent illumination: beyond weak object approximation," Photon. Res. **11**, 442–455 (2023).
4. D. Mason, J. Chen, M. Rossi, Y. Tsaturyan, and A. Schliesser, "Continuous force and displacement measurement below the standard quantum limit," Nat. Phys. **15**, 745–749 (2019).
5. Z.-Y. Zhou, D.-S. Ding, Y.-K. Jiang, Y. Li, S. Shi, X.-S. Wang, and B.-S. Shi, "Orbital angular momentum light frequency conversion and interference with quasi-phase matching crystals," Opt. Express **22**, 20298–20310 (2014).
6. Y. Li, H. Li, J. Huang, C. Fang, M. Liu, C. Huang, and G. Zeng, "High-precision temperature sensor based on weak measurement," Opt. Express **27**, 21455–21462 (2019).
7. B. Skinner, J. Ruhman, and A. Nahum, "Measurement-induced phase transitions in the dynamics of entanglement," Phys. Rev. X **9**, 031009 (2019).
8. C. Xu, L. Zhang, S. Huang, T. Ma, F. Liu, H. Yonezawa, Y. Zhang, and M. Xiao, "Sensing and tracking enhanced by quantum squeezing," Photon. Res. **7**, A14–A26 (2019).
9. N. Brunner and C. Simon, "Measuring small longitudinal phase shifts: weak measurements or standard interferometry?" Phys. Rev. Lett. **105**, 010405 (2010).
10. G. Wanner, "Space-based gravitational wave detection and how LISA pathfinder successfully paved the way," Nat. Phys. **15**, 200–202 (2019).
11. Y. Gong, J. Luo, and B. Wang, "Concepts and status of Chinese space gravitational wave detection projects," Nat. Astron. **5**, 881–889 (2021).
12. Y. Yin, Z. Liu, S. Jiang, W. Wang, H. Yu, W. Li, and Jirigalantu, "Grating-based 2D displacement measurement with quadruple optical subdivision of a single incident beam," Opt. Express **29**, 24169–24181 (2021).
13. T. Nagata, R. Okamoto, J. L. O'Brien, K. Sasaki, and S. Takeuchi, "Beating the standard quantum limit with four-entangled photons," Science **316**, 726–729 (2007).
14. P. Georgi, M. Massaro, K.-H. Luo, B. Sain, N. Montaut, H. Herrmann, T. Weiss, G. Li, C. Silberhorn, and T. Zentgraf, "Metasurface interferometry toward quantum sensors," Light Sci. Appl. **8**, 70 (2019).
15. L.-Z. Liu, Y.-Z. Zhang, Z.-D. Li, R. Zhang, X.-F. Yin, Y.-Y. Fei, L. Li, N.-L. Liu, F. Xu, Y.-A. Chen, and J.-W. Pan, "Distributed quantum phase estimation with entangled photons," Nat. Photonics **15**, 137–142 (2021).
16. I. Afek, O. Ambar, and Y. Silberberg, "High-NOON states by mixing quantum and classical light," Science **328**, 879–881 (2010).
17. P. Thomas, L. Ruscio, O. Morin, and G. Rempe, "Efficient generation of entangled multiphoton graph states from a single atom," Nature **608**, 677–681 (2022).
18. X.-L. Wang, L.-K. Chen, W. Li, H. L. Huang, C. Liu, C. Chen, Y. H. Luo, Z. E. Su, D. Wu, Z. D. Li, H. Lu, Y. Hu, X. Jiang, C. Z. Peng, L. Li, N. L. Liu, Y.-A. Chen, C.-Y. Lu, and J.-W. Pan, "Experimental ten-photon entanglement," Phys. Rev. Lett. **117**, 210502 (2016).
19. K. Otsuka, "Self-mixing thin-slice solid-state laser Doppler velocimetry with much less than one feedback photon per Doppler cycle," Opt. Lett. **40**, 4603–4606 (2015).
20. J. Li, H. Niu, and Y. X. Niu, "Laser feedback interferometry and applications: a review," Opt. Eng. **56**, 050901 (2017).
21. B. Liu, Y. Jiang, and H. Ji, "Sensing by dynamics of lasers with external optical feedback: a review," Photonics **9**, 450 (2022).
22. E. Lacot, B. Houchmandzadeh, V. Girardeau, O. Hugon, and O. Jacquin, "Nonlinear modification of the laser noise power spectrum

induced by frequency-shifted optical feedback," Phys. Rev. A **94**, 033843 (2016).
23. E. Lacot, R. Day, and F. Stoeckel, "Coherent laser detection by frequency-shifted optical feedback," Phys. Rev. A **64**, 043815 (2001).
24. V. Giovannetti, S. Lloyd, and L. Maccone, "Quantum-enhanced measurements: beating the standard quantum limit," Science **306**, 1330–1336 (2004).
25. P. Walther, J.-W. Pan, M. Aspelmeyer, R. Ursin, S. Gasparoni, and A. Zeilinger, "De Broglie wavelength of a non-local four-photon state," Nature **429**, 158–161 (2004).
26. M. W. Mitchell, J. S. Lundeen, and A. M. Steinberg, "Super-resolving phase measurements with a multiphoton entangled state," Nature **429**, 161–164 (2004).
27. D. G. England, B. Balaji, and B. J. Sussman, "Quantum-enhanced standoff detection using correlated photon pairs," Phys. Rev. A **99**, 023828 (2019).
28. S. Zhang, L. Yan, B. Chen, Z. Xu, and J. Xie, "Real-time phase delay compensation of PGC demodulation in sinusoidal phase-modulation interferometer for nanometer displacement measurement," Opt. Express **25**, 472–485 (2017).
29. X. Chen, M. E. Kandel, C. Hu, Y. J. Lee, and G. Popescu, "Wolf phase tomography (WPT) of transparent structures using partially coherent illumination," Light Sci. Appl. **9**, 142 (2020).
30. Y. Xu, X. Pan, M. Sun, W. Liu, C. Liu, and J. Zhu, "Single-shot ultrafast multiplexed coherent diffraction imaging," Photon. Res. **10**, 1937–1946 (2022).
31. M. Song, J. Steinmetz, Y. Zhang, J. Nauriyal, K. Lyons, A. N. Jordan, and J. Cardenas, "Enhanced on-chip phase measurement by inverse weak value amplification," Nat. Commun. **12**, 6247 (2021).
32. H. Li, W. Huang, W. Zhang, and J. Zhang, "Fiber optic strain rate sensor based on a differentiating interferometer," Photon. Res. **10**, 2599–2606 (2022).